Article

Molecular beacon-gold nanosensors for Leucine-rich alpha-2-glycoprotein-1 (Lrg1) detection in pathological angiogenesis

DANIEL CHIN SHIUAN LIO, CHENGHAO LIU, Christian Wiraja, Beiying Qiu, Chee Wai Fhu, Xiaomeng Wang, and Chenjie Xu

ACS Sens., **Just Accepted Manuscript** • DOI: 10.1021/acssensors.8b00321 • Publication Date (Web): 10 Aug 2018

Molecular beacon-gold nanosensors for Leucine-rich alpha-2-glycoprotein-1 (Lrg1) detection in pathological angiogenesis

Daniel Chin Shiuan Lio[1,2,3], Cheng Hao Liu[1,3], Christian Wiraja[1], Beiying Qiu[4], Chee Wai Fhu[3], Xiaomeng Wang[3,4,5,6*], Chenjie Xu[1,2*]

[1] School of Chemical and Biomedical Engineering, Nanyang Technological University, 70 Nanyang Drive, Singapore, 637457, Singapore.

[2] NTU-Northwestern Institute for Nanomedicine, Interdisciplinary Graduate School, Nanyang Technological University, 50 Nanyang Avenue, Singapore, 639798, Singapore.

[3] Lee Kong Chian School of Medicine, Nanyang Technological University, Singapore, 59 Nanyang Drive Singapore 636921

[4]Institute of Molecular and Cell Biology, Agency for Science, Technology and Research (A*STAR), Proteos, Singapore, 61 Biopolis Dr, Singapore 138673

[5]Singapore Eye Research Institute, The Academia, 20 College Road, Discovery Tower Level 6, Singapore 169856

[6]Institute of Ophthalmology, University College London, 11-43 Bath Street, London, UK, EC1V 9EL

* Correspondence to cjxu@ntu.edu.sg; wangxiaomeng@ntu.edu.sg

Keywords: Lrg1, Gold Nanoparticles, Angiogenesis, Molecular Beacon, Biosensor, mRNA detections

Abstract:

Leucine-rich alpha-2-glycoprotein-1 (Lrg1) is an emerging biomarker for angiogenesis. Its expression in ocular tissues is up-regulated in both human patients with proliferative diabetic retinopathy and rodent models of pathological angiogenesis. However, there is no existing sensor that allows visualization and monitoring of Lrg1 expression non-invasively and in real time. Herein, we report a nucleic acid-gold nanorod-based nanosensor for the non-invasive monitoring of cellular Lrg1 expression in angiogenesis. Specifically, this platform is constructed by covalently conjugating molecular beacons onto gold nanorods, which pre-quench the fluorophores on the molecular beacons. Upon intracellular entry and endosomal escape, the complexes interact with cellular Lrg1 mRNA through hybridization of the loop area of the molecular beacons. This complexation distances the fluorophores from nanorod and restores the pre-quenched fluorescence. The reliability of this platform is confirmed by examining the increased Lrg1 expression in migrating keratinocytes and the Lrg1 gene changes in different postnatal stages of mouse retinal vasculature growth in the mouse retina model.

Angiogenesis, a process of new blood vessel formation, contributes to the development and progression of several diseases including cancers, proliferative diabetic retinopathy, and chronic wound healing [1]. This complex process is regulated through a balance of proangiogenic and anti-angiogenic molecules, which is often derailed in diseases [2]. Repetitive monitoring of angiogenic gene expression patterns *in vivo* would allow the dynamic tracking of biological changes during disease progression or upon treatment [3].

Although vascular endothelial growth factors (VEGFs) and their receptors play a key role in angiogenesis [4-6], other factors also contribute to angiogenesis through extensive crosstalk with each other [7-9]. For example, TGF-β1 signaling has been reported to be involved in multiple steps during angiogenesis [10], and can promote or inhibit new blood vessel formation, which is highly dependent on factors, such as ligand concentration, its bioavailability, presence of other regulatory factors [11]. Our team et al. have discovered Leucine-rich alpha-2-glycoprotein 1 (Lrg1), as a promising therapeutic target in the diagnosis and treatment of angiogenesis-related diseases [12-13]. It was found to mediate vessel growth through regulating the endothelial TGFβ1 signaling.

The expression of Lrg1 in cells and animal models is currently examined through classic techniques such as reverse transcription polymerase chain reaction (RT-PCR), western blotting, and immunostaining [12, 14-15]. While they provide extremely sensitive and definitive validation, it comes with a major drawback in the need to sacrifice multiple animals to obtain statistically significant observation, as in the case for any end-point analysis methods. Therefore, it is always desirable to have a non-invasive and real-time imaging method for *in vivo* monitoring of Lrg1 expression, which could potentially relate to activation of angiogenic switch, leading to pathological angiogenesis in diseases.

In recent years, oligonucleotides-functionalized gold nanomaterials such as Spherical Nucleic Acids (SNAs) have surfaced as a reliable technique for the detection of the abnormal expression of disease biomarkers [16-22]. These biocompatible complexes can easily enter living cells through scavenger receptor-mediated endocytosis despite its negatively-charged surface [23], which can't be achieved by the pure oligonucleotide-based probes (e.g. molecular beacon). The oligonucleotides on the particles are resistant to nuclease degradation due to steric effect from their tight packing [24] and more importantly, they can detect and quantify cellular gene in nanomolar sensitivity [25-26]. SNAs have been used to sort aggressive melanoma cells within

heterogeneous cell lines via the detection of Nodal (a biomarker for tumor progression localized in vascular networks) re-expression in aggressive metastatic melanoma [27]. Such sorting can be achieved through the hybridization of designed oligonucleotide and complementary Nodal mRNA sequence, releasing fluorescence signals within the cell which are detectable through fluorescence imaging. To allow more precise detection of biomarkers, these nanoparticles could be multiplexed with target gene and control sequence to improve cell sorting and quantification[28-31]. In addition, SNAs demonstrated great cellular penetration of >100% in skin keratinocytes within hours, accompanying effective suppression of epidermal growth factor receptor (EGFR) with EGFR siRNA-conjugated SNAs which led to reduction of epidermal thickness by almost 40% in mouse; without detectable toxicity [17].

Based on these pioneering works, we hypothesize that oligonucleotide-gold complexes would also allow the non-invasive and real-time monitoring of cellular Lrg1 expression for the diagnosis of pathological angiogenesis. As a proof-of-concept, we built one model system by complexing molecular beacons (MB) with gold nanorod (Figure 1). MBs, single stranded hairpin shaped oligonucleotides, with only one fluorophore are specifically designed to recognize the exon sequences of Lrg1 mRNA. They are conjugated onto gold nanorods through thiol-gold bond. [22, 32]. The complexation brings the dyes in close proximity with the gold nanorods, resulting in its quenching. Gold nanorods exhibit intense and narrow optical absorption peaks in the far-red and near-infrared (NIR) wavelength regions, owing to the excitation of longitudinal plasmons. This further permits the use of NIR dyes for a deep tissue penetration. In addition, gold nanorods are recently discovered to be a good contrast agent for photoacoustic imaging, a rapidly emerging biomedical imaging modality with functional imaging information at clinically-relevant penetration depths, while maintaining high spatial resolution and signal contrast [33]. It provides the potential utilization of multimodality imaging in the future for more comprehensive analysis. The synthesized complexes are approximately 68 nm in diameter with quenching efficiency greater than 90%. Their specificity towards the Lrg1 mRNA is first examined with *in vitro* keratinocytes before *ex vivo* application on mouse retina models.

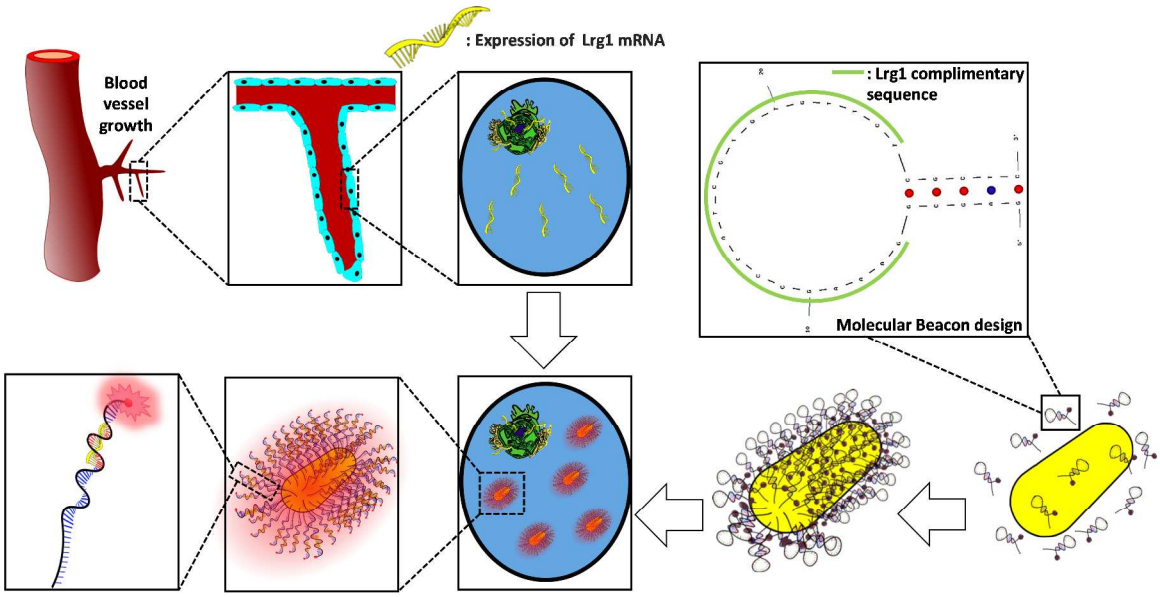

Figure 1: Schematic diagram of molecular beacon-gold nanorod complex-based biosensors for the non-invasive detection of the angiogenesis biomarker, Lrg1 in pathological angiogenesis. (Top left, clockwise): the nanosensors are designed as a potential diagnostic tool for pathological angiogenesis. In particular, abnormal blood vessel growth which results from high Lrg1 expression in the endothelium cells lining the blood vessels. Upon uptake of nanosensors into the cells, Lrg1 mRNA will bind to the complementary molecular beacon strands on these sensors. The binding will displace the fluorophore from the gold nanoparticle, leading to the restoration of fluorescence. Therefore, the fluorescence intensity feedback could potentially reflect the regulation of Lrg1 expression.

Experimental Section

MB design and preparation: MB was designed using IDT's OligoAnalyzer Tool. An 18-atom hexa-ethyleneglycol spacer (iSP18) was designed to hold together the loop sequence and thiolated group (Table S1). A short 20 base sequences were designed to be complimentary to Lrg1 mRNA exon sequences, with an expect value of 0.017 (human) and 0.008 (mouse). Oxidized (disulfide) MB (Integrated DNA Technologies) were chemically reduced by Dithiothreitol (DTT) to form thiolated MB. Briefly, 8µl of 100µM MB was mixed with 3.2µl of 0.1M DTT in 400 µl RNAse and DNAse-free water for 1 hour at room temperature. DTT was then removed using NAP-5 Columns (GE Healthcare Life Sciences).

Complexation of Gold nanorods and MBs: Citrate-capped gold nanorods (25nm, absorbance 550 nm, Sigma-Aldrich) were filtered with 0.2 μm syringe filter to remove any aggregate or bacteria. Later, 3 μL 1% Tween 20 (Bio-Rad) was added to the 0.3mL aqueous solution containing 13.5 μg gold nanorods and the whole solution was vortexed for 10 mins. The solution was added to reduced thiolated MBs (2μM) and left for 1 hour at room temperature. Next, the solution was salt-aged with 5M NaCl in water to achieve concentrations of 0.05, 0.1, 0.2, 0.3, 0.4, 0.5M over a period of 3 hours. After every addition of salt solution, the molecular beacon-gold nanorods solution was sonicated for 10 seconds. Finally, excess MBs were removed through centrifugation at 15,000rpm at room temperture for 30 minutes. The final complexes were suspended in 100 μL PBS with 0.01% Tween-20.

Cell labeling with Lrg1 MB-gold nanorod nanosensors: HaCaT cells (both untreated and Lrg1 silence) were labeled with 1.8 μg of Lrg1 MB-gold nanorods in 1ml Opti-MEM medium. As a control, cells were also labeled with scramble MB-gold nanorods. The cells were then left in the incubator for 4 hours, washed once with PBS to remove the excessive scramble MB-gold nanorods, followed by fixation in formalin solution (Sigma) for 10mins. Formalin was then removed and replaced with PBS for fluorescence imaging. RT3 cells (carcinoma squamous cells) were also labeled in the similar way to serve as a control.

Cell Scratch Assay: 0.6 x 10^6 cells of HaCaT were seeded onto one well of a 6-well culture plate. 1 day later, a 200μl pipette tip was used to create a cross scratch in the well. Cells were then washed with complete DMEM once and examined for proliferation rate by observing cell closure at 0, 12, 24, 30, 35hrs. For Lrg1 MB-gold nanorods labelling, cells were treated at 12 hours with 1.8 μg of nanosensors for 4 hours before fluorescence imaging. For immunofluorescence staining, HaCaT cells were fixed with 4% PFA and blocked with PBS containing 0.5% BSA, 1% Tween 20, and 1.5% Triton X-100 for 1 hour before being incubated with primary antibodies against LRG1 (Proteintech Group, USA,13224-1-AP) overnight at room temperature and identified with Alexa Fluor® 488 and DAPI.

Lrg1 staining in mouse retina: All procedures were performed in accordance to IACUC (#140963) of Nanyang Technological University. Briefly, mouse retina from wild-type C57BL/6 (adult, postnatal 15 and 5 days) was isolated as described elsewhere [34]. To prevent retina from curling, 6-well plates were pre-coated with Aquaphor®. Retinas were then labeled with 5.4 μg of MB-gold nanorods in 100μL of Endothelial Growth Basal Medium (EBM-2). Concurrently, MBs (without gold nanorods) were also delivered using Lipofectamine 3000 into the mouse retina. After 4 hours of incubation, the tissues were washed with PBS three times to remove excess nanorods, followed by formalin fixation, and carefully placed on glass slides for fluorescence imaging. To determine if the locality of nanosensors coincided with retina vasculature, immunostaining was performed with CD31 (BD Pharmingen) and IB4 (Vector Laboratories) (established markers for blood vessels [35-36]) after incubation with gold nanorods. Briefly, retina labeled with nanorods was fixed with methanol for 2 hours. Retina was then washed three times with PBS, followed by incubating in blocking buffer for 1hr at room temperature. Primary antibody (CD31 or IB4) were diluted 1:200 and 1:100 respectively in blocking buffer before incubating with retina samples overnight at 4°C. Next, samples were washed with blocking buffer for six times, before incubating with secondary antibody (Alexa Fluor® 488, Thermo Fisher), 1:200 dilution in blocking buffer. Excess antibodies were then removed by washing with blocking buffer six times. Finally, samples were placed carefully on glass slides with ProLong Gold Antifade Mountant (Thermo Fisher) for fluorescence imaging.

Results and Discussion

Design, synthesis and characterization of Lrg1 MB-gold nanorod complexes

Sequence similarity searching with Basic Local Alignment Search Tool (BLAST) showed that the 1233-1252 bp of mouse LRG1 mRNA sequence and the 1514-1533 bp of human LRG1 mRNA sequence are highly specific to human and mouse Lrg1 mRNA (SI Figure S1). To create a loop structure, stem sequences are introduced (Table S1), and molecular beacon is stable as depicted by IDT Oligo Analyzer, with close ΔG values of -2.82 kcal/mole (human) and -2.81 kcal/mole (mouse).

Gold nanorods are selected because of their near-infrared absorption which facilitates imaging on deeper tissues. These unmodified gold nanorods had a longitudinal length of

52.6±0.8 nm and a transverse width of 34.2±1.0nm (SI Figure S2). The most critical question during the complexation step through gold-sulphur bond was whether gold nanorods were able to effectively quench the fluorescence of the dye (i.e. Cy3) on the MBs. As shown in Figure 2A, the absorbance of gold nanorods overlaps well with the Cy3 fluorescence emission. To examine the actual quenching efficiency, a range of gold nanorods solutions were modified with the Lrg1 MB solution at a fixed MB concentration. As shown in Figure 2B (black line), the fluorescence was strongest when the ratio of MB against gold nanorods was above 8,000. However, a gradual increase of the gold nanorods in the synthesis (i.e. a gradual decrease of the MB/gold nanorods ratio) led to a decrease of fluorescence, with the maximal quenching of 95% fluorescence intensity observed at 1,500 MBs per gold nanorod. Next, we fixed the concentration of gold nanorods while tuning the MB concentration in the synthesis. As shown in Figure 2B (red line), there was negligible fluorescence when the MB/gold nanorod ratio was below 1,500 until a spike increase in fluorescence intensity showed up when the ratio was 1500, suggesting that excess unbound MB was present in the mixture. Therefore, we conclude that the average number of MBs per gold nanorods should be around 1,500 which is comparable to the previous report from [37], demonstrating a DNA coverage of ~1200 strands per 50 nm spherical gold nanoparticle. One direct consequence of this MB coating is the increase of hydrodynamic diameters of the particles (Figure 2C). The size increased from 52 nm to 65 nm in dynamic light scattering. EDX analysis showed the Phosphorus peak surrounding the gold nanorods, indicating the presence of oligonucleotides (Figure 2D). One thing to note is that the longitudinal and transverse peaks were not differentiated in DLS, which was due to the low aspect ratio of gold nanorods used here. Therefore, it is confirmed through the quenching of MB fluorescence, increase of nanorod hydrodynamic diameter, and EDX that MBs are conjugated successfully onto nanorods.

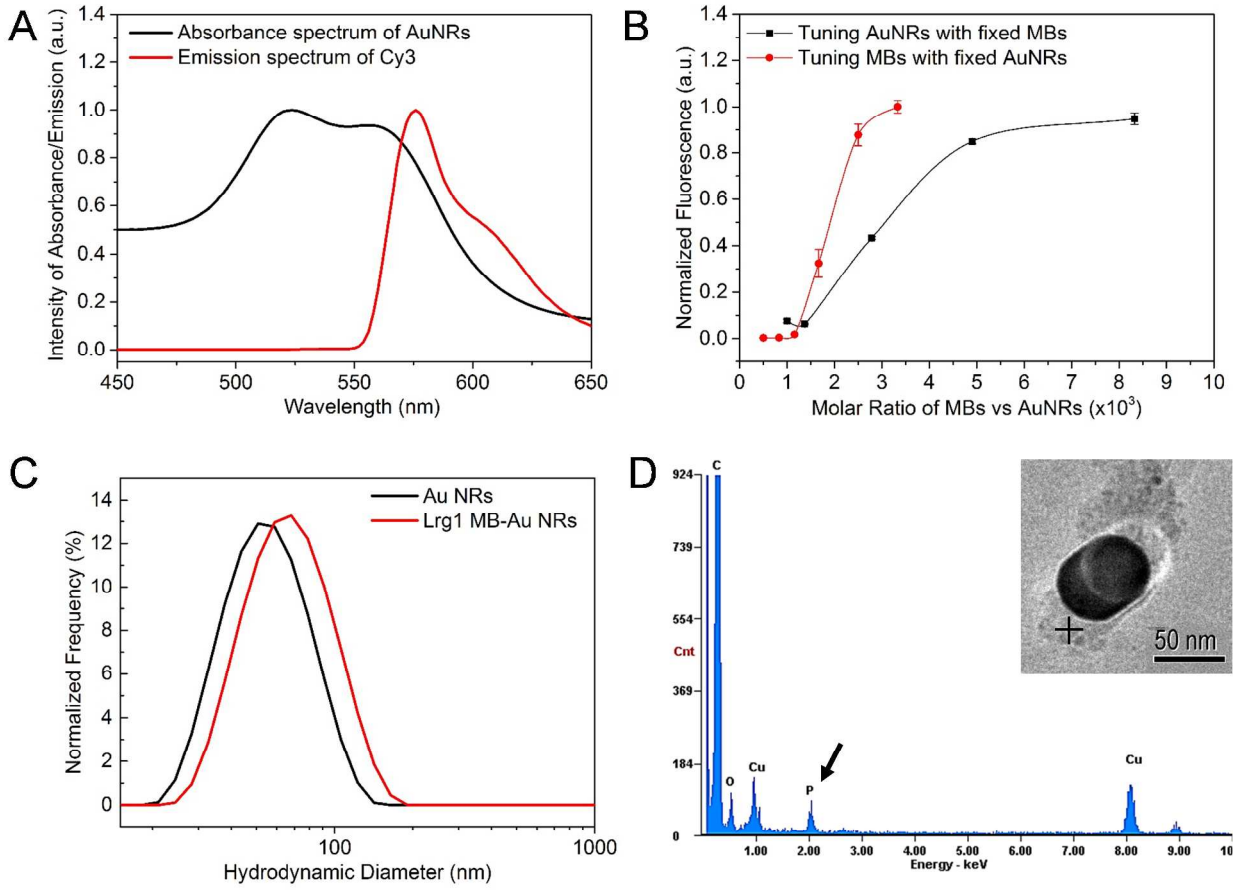

Figure 2: Characterization of Lrg1 MB-gold nanorod complexes. (**A**) UV-VIS absorbance spectrum of gold nanorods and fluorescence emission of Cy3-labelled MBs. (**B**) The quenching effect during the complexation of MBs and gold nanorods. (**C**) Hydrodynamic diameters of gold nanorods before and after the complexation with MBs. (**D**) Energy Dispersive X-ray analysis for Transmission Emission Microscope image of Lrg1 MB-gold nanorod complex shows the presence of Phosphorus (a component of DNA) as indicated with black arrow.

Next we determined the specificity of the complexes towards Lrg1 complementary short sequence. We mixed either Lrg1 MB-gold nanorods (stated as Nanosensors) or scramble MB-gold nanorods (stated as Mismatched Nanosensors) with Lrg1 complementary short sequence or the scrambled sequence. As shown in Figure 3A, there was ~50% increase of fluorescence in 30 minutes only when the Lrg1 MB-gold nanorods were mixed with Lrg1 complementary short sequence. It is expected to be the result of distancing the dyes from the gold nanorods upon the binding of Lrg1 complementary short sequence and MBs. No fluorescence restoration was

observed when scrambled sequence was added instead. In addition, scramble MB-conjugated gold nanorods could not be activated by neither Lrg1 complementary short sequence nor the scrambled sequence (Figure 3B).

The sensitivity of this probe was examined with a range of Lrg1 complimentary short sequence concentrations, in which 0.25 μM Lrg1 sequence was sufficient to trigger a 40% increase of fluorescence within 30 minutes (SI Figure S3A). Furthermore, a study was performed to study the limit of detection for these nanosensors. A linear relationship was observed between 0.01 and 0.25 μM (SI Figure S4). Last but not least, despite saturating scramble MB-gold nanorods with 2μM of Lrg1 complimentary short sequence, no detectable change in fluorescence intensity was observed (SI Figure S3B).

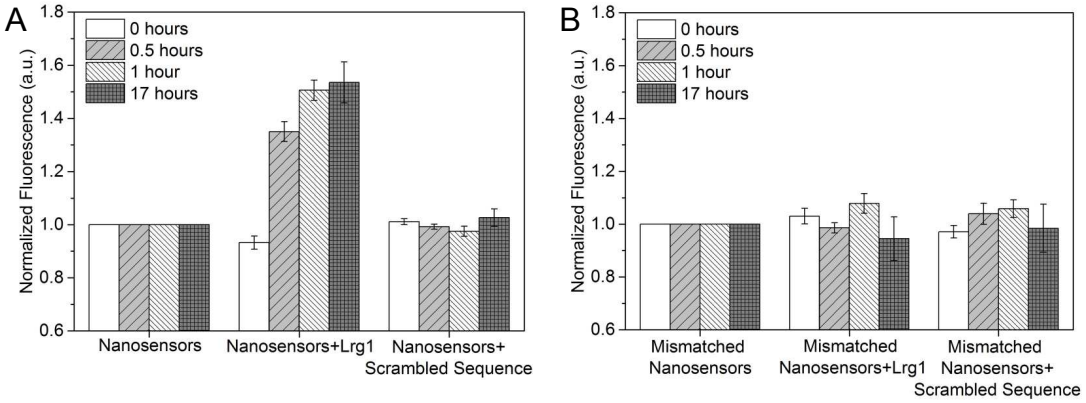

Figure 3: The specificity of Lrg1 MB-gold nanorod nanosensors against Lrg1 complementary strands. Fluorescence restoration of (**A**) Lrg1 MB-gold nanorods and (**B**) scramble MB-gold nanorods before and after the introduction of Lrg1 short sequence over a period of 17 hrs. All values are mean ± SD, n=3.

***In vitro* testing of Lrg1 MB-gold nanorod cytotoxicity and penetration in mammalian cells**

The cytotoxicity of MB-gold nanorod complexes was examined through MTS cell proliferation assay in HaCaT keratinocyte cells. The concentration of the complexes was tuned between 0.45 μg/ml and 2.7 μg/ml. As shown in SI Figure S5, any concentration below 1.8 μg/ml did not significantly affect the cell viability. Interestingly, the unmodified gold nanorods had negatively influenced the cell viability under the same concentration. This difference could be caused by the cytotoxicity of aggregated unmodified gold nanorods in cells [38-39]. In the following *in vitro* experiments, the MB-gold nanorods' concentration was controlled below 1.8 μg/ml.

The cellular uptake was also studied by incubating HaCaT cells with 1.8 μg/ml complexes for 4 hours. As shown in Figure 4A, this incubation caused most of the cells to become fluorescent with Cy3 MB fluorescence surrounded the nuclei (blue). Flow cytometry further revealed that 40% cells were successfully labeled (positive for Lrg1) (SI Figure S6). Meanwhile only 7.52% cells (a negligible subpopulation) were found to exhibit Cy3 fluorescence, when labelled with scramble MB-gold nanorods. To confirm the location of the nanosensors, we labeled the cell membrane with lipophilic fluorescent dye (DiO). As shown in Figure 4B, red signal from nanosensors was mainly present within the green membrane boundary. It is also notable to mention that red signal was negligibly found in the cell nucleus.

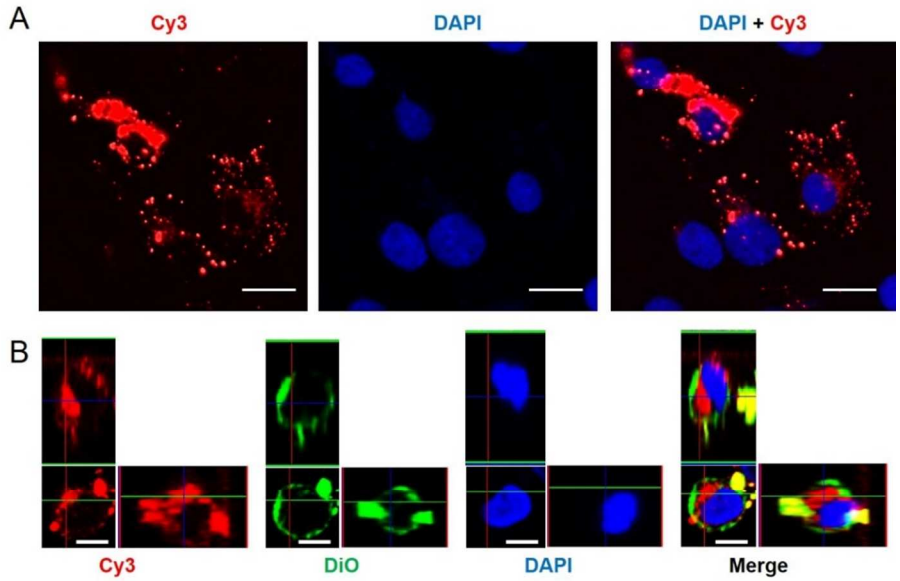

Figure 4: Cellular localization of Lrg1 MB-gold nanorods. (**A**) Fluorescence images of HaCaT cells labeled with Lrg1 MB-gold nanorods. (**B**) Confocal image of a HaCaT cell. Red (Lrg1 MB-gold nanorods), blue (nucleus), green (plasma membrane), and merged image (red + green + blue). (Scale bar represents 10 μm)

The cytotoxicity test confirms the safety of the MB-gold nanorods while the cellular uptake experiments reveal their capability of entering cell cytoplasm through endocytosis and thereafter residing in cell cytoplasm for mRNA detection. Next, we evaluate the functionality of the MB-gold nanorods in detecting the Lrg1 mRNA expression in cells.

Cells were split into three treatment groups. The first group were treated with Lrg1 MB-gold nanorods directly. The second group were treated with Lrg1 siRNA to silence any Lrg1

gene before being labeled with Lrg1 MB-gold nanorods. The third group were treated with scramble MB-gold nanorods. After 4 hours, fluorescence signal in group 2 was ~50% lower than group 1 (Figure 5A & B). Similarly, fluorescence signal in group 3 was ~75% lower than group 1. To confirm this observation, the cellular Lrg1 mRNA in three groups was quantified through RT-PCR (Figure 5C). Lrg1 mRNA expression was found to be ~80% lower in Lrg1 silenced cells when being compared to the untreated cells. Thus, Lrg1 mRNA expression is well-represented by Lrg1 MB-gold nanorods signal.

Besides the differentiation of Lrg1 gene expression in HaCaT cells under normal and Lrg1-silenced conditions, Lrg1 MB-gold nanorods were also able to differentiate Lrg1 gene expression across different cell lines. For example, RT3, a malignant keratinocyte cells have lower Lrg1 expression as compared to normal cells (HaCaT). Under the same labeling condition, higher fluorescence signal was observed in HaCaT cells (SI Figure S7A) and almost 9 times of that in RT3 cells (SI Figure S7B). RT-PCR analysis revealed the Lrg1 gene expression in RT3 cells was only 20% of that in HaCaT cells (SI Figure S7C). Therefore, our nanosensors allowed the differentiation of the normal keratinocytes (HaCaT cells), HaCaT cells silenced with Lrg1 siRNA, and RT3 (Figure 5& SI Figure S7).

In a separate *in vivo* experiment (Supplementary results only for reviewers), this Lrg1 MB-gold nanorod sensor demonstrated the ability to label and detect the keratinocyte cells in the skin epidermis layer of the mouse. This is on par with our *in vitro* findings (Figure 4&5), demonstrating high expression of Lrg1 mRNA in HaCaT cells using Lrg1-targeted nanosensor. On the other hand, skin applied with scramble MB-gold nanorods showed minimal signal in the epidermal layer.

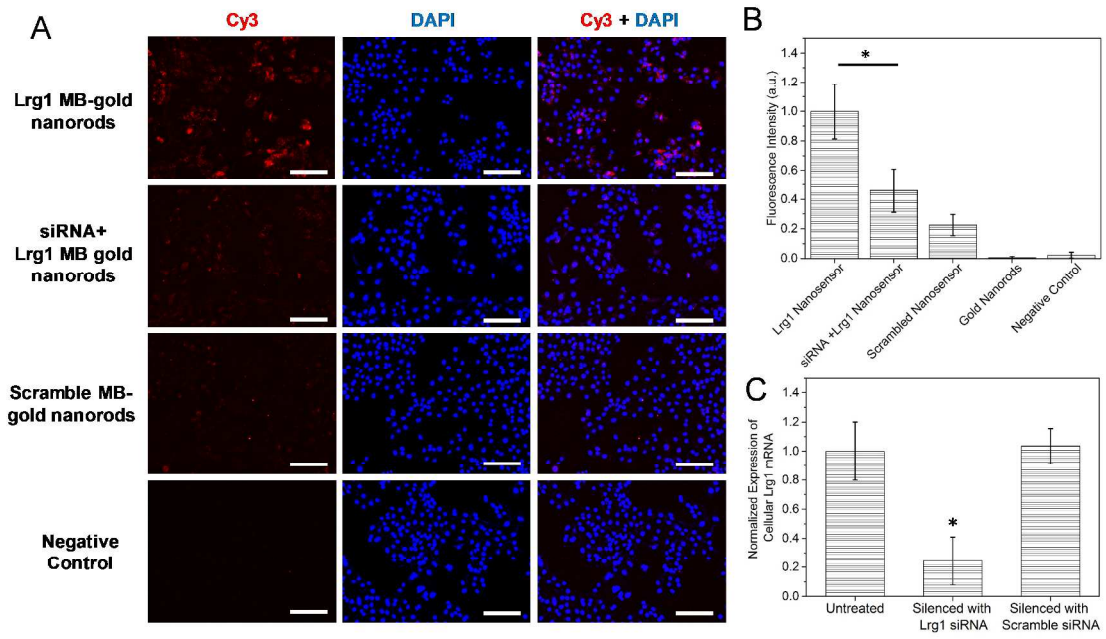

Figure 5: Lrg1 MB-gold nanorods monitor gene regulation in keratinocytes. (**A**) Representative fluorescence images of normal and Lrg1-silenced HaCaT cells labelled with Lrg1 MB-gold nanorods, and cells labelled with scramble MB-gold nanorods. (**B**) Fluorescence signal quantification from (A) using ImageJ analysis. (**C**) RT-PCR analysis of Lrg1 gene in untreated, Lrg1 silenced and control silenced HaCaT cells, normalized against GAPDH. All values are mean ± SD, N≥3. Scale bar represent 100 µm. *p<0.05

Monitoring Lrg1 mRNA expression in *in vitro* wound healing model with Lrg1 MB-gold nanorods

Cell scratch assay is a convenient *in vitro* wound healing model. Here, Lrg1 MB-gold nanorods were used to examine the dynamic expression of Lrg1 in HaCaT cells in the healing model. To ensure constant imaging of similar area, scratch areas were marked with a scratch using a blade; this served as a reference to image the same area of cells over time. As shown in Figure 6A, the initial scratched area at 0 hour was displayed in light blue. Cell migration could be observed within 12 hours and an almost complete closure was observed by 30 hours. We labeled the cells with both sequence MB-gold nanorods for 12 hours after inducing the scratch. To note, the presence of MB-gold nanorods did not inhibit cell migration and closure. As shown in Figure 6B, ~50% higher fluorescence could be observed in cells at the scratched area as compared to cells in unscratched area (SI Figure S8A). This is indicative of Lrg1 upregulation when

keratinocytes underwent migration during wound healing process [14, 40]. To confirm this observation, immunostaining of Lrg1 protein was performed on the cells (Figure 6C). A 2-fold increase in fluorescence was observed for HaCaT cells at the scratched area as compared to HaCaT cells at the unscratched area (SI Figure S8B).

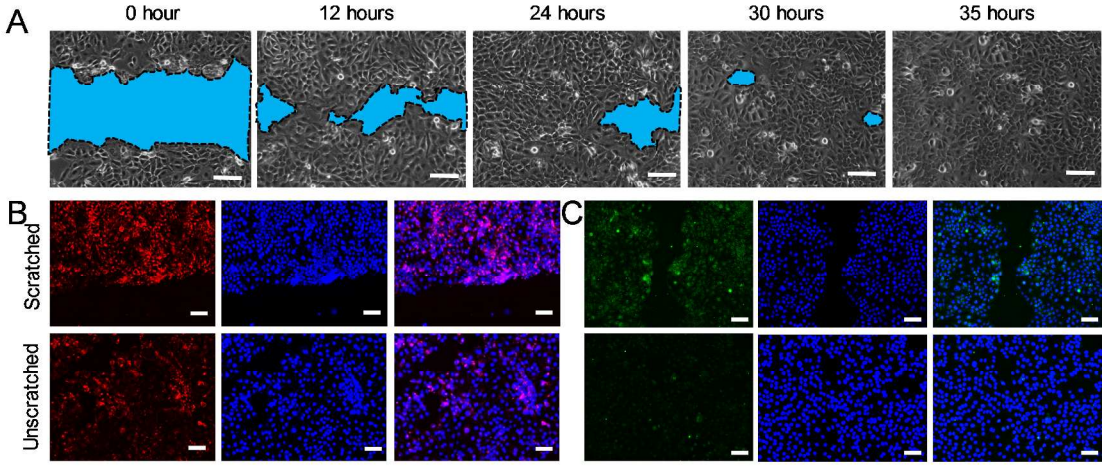

Figure 6: Lrg1 upregulation in HaCaT cells in the wound healing model. (**A**) Representative images of HaCaT cells in an *in vitro* wound healing model (scratch assay) – blue indicates the area without cells; (**B**) Representative fluorescence images of HaCaT cells at the scratched or un scratched areas after being labelled with Lrg1 MB-gold nanorods (red); (**C**) Immunostaining of Lrg 1 proteins in HaCaT cells at the wounded or untouched areas. Red (Lrg1 MB-gold nanorods), blue (nucleus), green (immunostaining of Lrg 1 proteins). (Scale bar represents 100 μm)

Lrg1 detection with Lrg1 MB-gold nanorods in *ex vivo* mouse retina model

Recently, we have discovered that the expression of Lrg1 would be upregulated during retinal vascular remodeling [12]. Moreover, studies showed time course illustration of retinal vascular development in C57BL/6 mice with endothelial cells immunostaining, whereby superficial vascular plexus were observed during first week after birth, Postnatal 1 (P1) – P3, and radial outgrowth of vessels from the optic nerve into the periphery and retinal edges were observed from P4 – P8 [41].

Figure 7A is a Rottermann contrast image of a removed C57BL/6 mouse retina right after separation from choroid. In Figure 7B, extracted retinas were placed in endothelial basal medium and labeled with Lrg1 MB-gold nanorods before being immunostained with blood vessels

specific biomarker CD31. Here, CD31 is used to specifically stain intercellular junction of endothelial cells. To study if gold nanorods are good gene carrier for retina tissue, molecular beacons (MBs) with similar sequences (gold nanorod was replaced by a dark quencher, sequence found as "Mouse Lrg1 MBs with dark quencher" in Table S1) were transfected using lipofectamine. Approximately 4 times higher Lrg1 gene detection can be observed with gold nanorods (Figure 7B & SI Figure S9); and upon closer look at the stained retina at high magnification, signals from Lrg1-MB gold nanorods aligned well with signal from CD31 (SI Figure S10). This implies that cells alongside blood vessels in the same layer of retina may also express Lrg1 gene. Next, we studied the specificity and stability of Lrg1 MB-gold nanorods in an *ex vivo* model by introducing scramble MB-gold nanorods into the retina. It can be observed that no fluorescence was recovered in retina labeled with scrambled MB-gold nanorods (SI Figure S11), indicating that MBs were still attached to gold nanorods, with Cy3 fluorescence remained quenched.

The location and biodistribution of Lrg1 MB-gold nanorods could be identified from the image of sectioned retinas (Figure 7C). DAPI signals (blue) indicate the presence of three major layers in retina including Ganglion cell layer (GCL), Inner nuclear layer (INL), and Outer nuclear layer (ONL). IB4 was used to specifically stain endothelial cells. Most nanosensors (red) resided in areas close to ganglion cell layer (GCL), where blood vessels were found. We also observed that few red signals were in INL, which overlapped with IB4. This indicates the presence of endothelial cells in this layer.

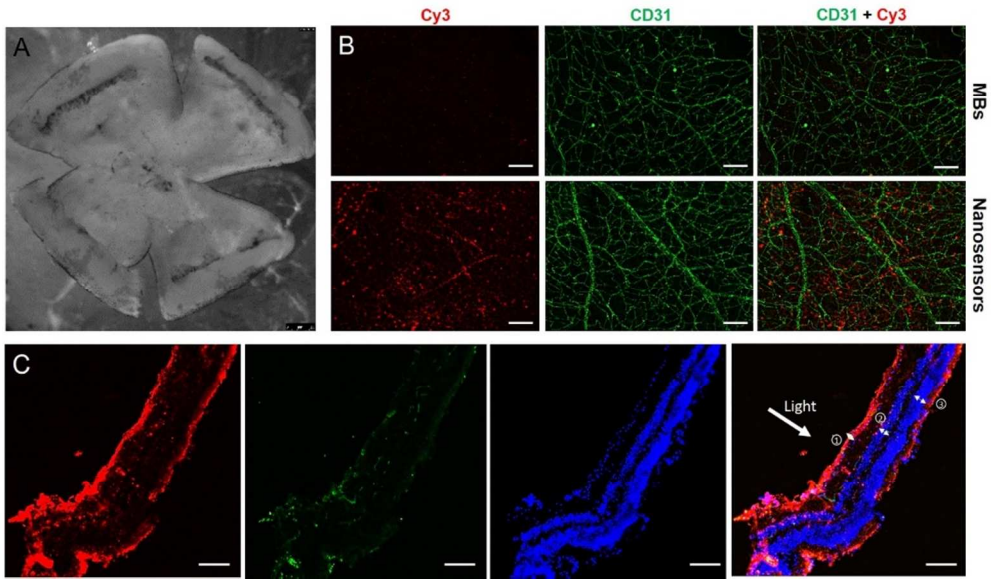

Figure 7: Lrg1 nanosensors for the analysis of Lrg1 expression in mouse retinal vascular. (**A**) Rotterman contrast image of the freshly collected mouse retina. (**B**) Fluorescence image of mouse retina labelled with pure Lrg1 MB (1st row) and Lrg1 nanosensors (2nd row). Both groups were stained with the blood vessels specific biomarker CD31 (green). (**C**) The sectioned mouse retina that has been labelled with Lrg1 nanosensors (red), IB4 which stains for endothelial cells (green) and DAPI (blue). The three major layers in retina include 1) Ganglion Cell Layer (GCL), 2) Inner Nuclear Layer (INL), and 3) Outer Nuclear Layer (ONL). Scale bar represents 100 μm.

Finally, to fully reveal the ability of Lrg1 MB-gold nanorods to detect Lrg1 gene regulation in mouse retina, we studied Lrg1 gene expression in different early postnatal stage mouse retina (P5, P15 and adult). The differences in Lrg1 expression in different postnatal stages have been demonstrated in [12] where an increase in Lrg1 is observed with increase postnatal stage. The vascular growth in adult and P15 retina would have reached the retinal edges, whereas P5 retina would demonstrate vascular outgrowth only in the periphery region [41]. Among all stages, there is no noticeable difference of cell number (Figure 8, nucleus staining). On the other hand, Lrg1-MB gold nanorods labeling in these retinas showed clear distinction in fluorescence signal (i.e. both intensity & pattern). The highest fluorescence intensity can be observed in the ascending order of P5 (0.14 a.u.), P15 (0.58 a.u.), followed by adult mouse retina (0.80 a.u.) (SI Figure S12). These studies confirm Lrg1 MB-gold nanorods ability to transfect mouse retina efficiently, with non-invasive monitoring of Lrg1 gene expression. While the nanosensor showed great potentials in detecting Lrg1 mRNA in various models, there are questions left to answer.

Firstly, the nanosensor's sensitivity remains a challenge. While the overlap of gold nanorods' absorption spectrum and Cy3 fluorophore emission coincides (Figure 2A), slight background fluorescence remains. Distinct gold nanoparticle morphology could be adapted for improved quenching, besides optimization of beacon probe length. And it is also possible to shorten the distance between gold nanorod fluorescence, leading to stronger fluorescence quenching. Secondly, it is of importance to study gold nanorods uptake in the different cell lines studied. Possible studies in the future include silver staining to quantify the MB-gold nanorods uptake [42]. Thirdly, mechanism allowing nanosensors' penetration into the top two retinal layers (including GCL and INL) remains unclear. As the retina used in this experiment was fresh, the penetration should be attributed to the particles themselves. In the future, *in vivo* experiment on live mice will be carried to confirm this phenomenon before we further study the mechanism.

Finally, the Lrg1 MB-gold nanorod signal did not fully overlay with blood vessels-specific biomarker (i.e. CD31) signal (Figure 7B, SI Figure S10). This could be due to heterogenous penetration/ distribution of the nanosensors in the tissue. Some interaction between the ECM and nanosensors likely have convoluted its expression profile as well. In the future, daily "eye drops" application over a time period (e.g. 1 week) will be performed, to improve nanosensors distribution and thereby penetration into endothelial cell lining. Last but not least, it remains a question whether the developed nanosensor's detection limit is able to achieve an early diagnosis of pathological angiogenesis. In the future, *in vitro/ in vivo* studies can be performed to study the Lrg1 copy number in individual cells (both healthy and pathological state) and correlate it to the nanosensor's detection limit.

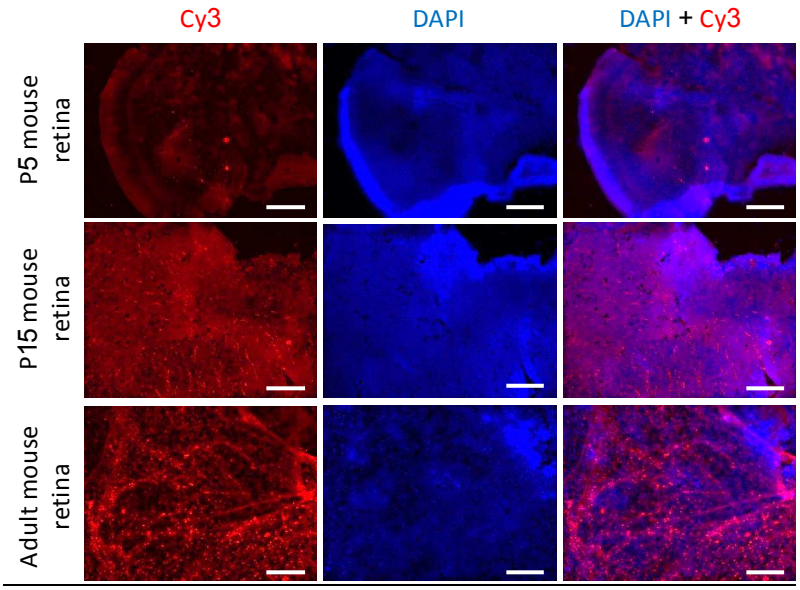

Figure 8: Representative fluorescence images of Lrg1 expression in different developmental postnatal stages of mouse retinal vascular. Red represents Lrg1 MB-gold nanorods, and blue represents nucleus. (Scale bar represent 100μm)

Conclusion

This article reports the design, synthesis, characterization, and utilization of the Lrg1 mRNA nanosensors for the noninvasive, real-time monitoring and verification of angiogenic biomarker Lrg1. This sensor is constructed by conjugating MBs onto the gold nanorods, which pre-quenches the MB fluorescence. As target mRNA hybridizes with the sensor, the straightening of

MB structure separates the fluorophore from gold nanorod and restores its fluorescence. The nanosensors were tested with target sequences, skin keratinocytes under various conditions, and mouse retina tissue. In all circumstances, it showed consistent performance in revealing the dynamic changes of Lrg1 expression without the need of additional cell/tissue disruption. We believe this nanosensor will pave the way to examine and monitor the development of angiogenesis in a real time manner.

Acknowledgement

This work is supported by NTU-Northwestern Institute for Nanomedicine (M4081502.F40 to C.J.X.), LKC-SCBE Collaborative Grant, and National Medical Research Council Singapore Cooperative Basic Research Grant (NMRC/CBRG/0058/2014 to X.M.W.).

Author contributions

The manuscript was written through contributions of all authors. All authors have given approval to the final version of the manuscript. Specifically, D.C.S.L., X.M.W. and C.J.X. conceived the project and wrote the manuscript. D.L. performed synthesis and characterization of nanosensor. D.C.S.L., L.C.H., C.W., B.Q., and F.C.W. performed cell culture, *in vivo* and *ex vivo* experiments. D.C.S.L., X.M.W., and C.J.X. wrote the manuscript.

Conflict of Interest

The authors declare no conflict of interest.

Supporting Information Available: The following files are available free of charge.

Supplementary Information for "Molecular beacon-gold nanosensors for Leucine-rich alpha-2-glycoprotein-1 (Lrg1) detection in pathological angiogenesis"

Brief description of contents:

Experimental Section; Nucleotide sequences used in *in vitro* and *ex vivo* experiments; Human and Mouse Lrg1 mRNA sequences; Transition electron microscope image; Fluorescence intensity recovery in the presence of different Lrg1 short sequence concentration; Limit of detection for Lrg1 MB-gold nanorods; Cytotoxicity of Lrg1 MB-gold nanorods; Fluorescence-

activated cell sorting; Lrg1 detection using nanoparticles in HaCaT vs RT3; Quantification of fluorescence signal in cell scratch assay model; High magnification fluorescence image of retina vasculature stained with CD31 (green) and Lrg1 MB-gold nanorods (red); Comparison of fluorescence signal quantification between Lrg1 MB-gold nanorods and scramble MB-gold nanorods in mouse retinal vasculature.; Quantification of fluorescence signal for Postnatal 5, Postnatal 15, and adult mouse retina.; Inkscape drawing of molecular beacon attachment onto gold through through gold-thiol bond, for non-invasive detection of Lrg1.

Reference

1. Carmeliet, P., Angiogenesis in life, disease and medicine. *Nature* **2005,** *438* (7070), 932-936.
2. Johnson, K. E.; Wilgus, T. A., Vascular Endothelial Growth Factor and Angiogenesis in the Regulation of Cutaneous Wound Repair. *Advances in Wound Care* **2014,** *3* (10), 647-661.
3. Barrett, T.; Brechbiel, M.; Bernardo, M.; Choyke, P. L., MRI of tumor angiogenesis. *Journal of magnetic resonance imaging : JMRI* **2007,** *26* (2), 235-49.
4. Leung, D. W., Cachianes, G, Kuang, W. J, Goeddel, D. V, Ferrara, N, Vascular endothelial growth factor is a secreted angiogenic mitogen. *Science (New York, N.Y.)* **1989,** *246* (4935), 1306-9.
5. Carmeliet, P., Ferreira, V., Breier, G., Pollefeyt, S., Kieckens, L., Gertsenstein, M., Fahrig, M., Vandenhoeck, A., Harpal, K., Eberhardt, C., Declercq, C., Pawling, J., Moons, L., Collen, D., Risau, W., Nagy, A., Abnormal blood vessel development and lethality in embryos lacking a single VEGF allele. *Nature* **1996,** *380* (6573), 435-9.
6. Ferrara, N., Carver-Moore, K., Chen, H., Dowd, M., Lu, L., O'Shea, K. S., Powell-Braxton, L., Hillan, K. J., Moore, M. W., Heterozygous embryonic lethality induced by targeted inactivation of the VEGF gene. *Nature* **1996,** *380* (6573), 439-42.
7. Holderfield, M. T.; Hughes, C. C., Crosstalk between vascular endothelial growth factor, notch, and transforming growth factor-beta in vascular morphogenesis. *Circulation research* **2008,** *102* (6), 637-52.
8. Chung, A. S.; Ferrara, N., Developmental and pathological angiogenesis. *Annual review of cell and developmental biology* **2011,** *27*, 563-84.
9. Carmeliet, P.; Jain, R. K., Molecular mechanisms and clinical applications of angiogenesis. *Nature* **2011,** *473* (7347), 298-307.
10. Viñals, F.; Pouysségur, J., Transforming Growth Factor β1 (TGF-β1) Promotes Endothelial Cell Survival during In Vitro Angiogenesis via an Autocrine Mechanism Implicating TGF-α Signaling. *Molecular and Cellular Biology* **2001,** *21* (21), 7218-7230.
11. ten Dijke, P.; Arthur, H. M., Extracellular control of TGF[beta] signalling in vascular development and disease. *Nat Rev Mol Cell Biol* **2007,** *8* (11), 857-869.
12. Wang, X., Abraham, Sabu, McKenzie, Jenny A. G., Jeffs, Natasha, Swire, Matthew, Tripathi, Vineeta B., Luhmann, Ulrich F. O., Lange, Clemens A. K., Zhai, Zhenhua, Arthur, Helen M., Bainbridge, James W. B., Moss, Stephen E., Greenwood, John, LRG1 promotes

angiogenesis by modulating endothelial TGF-[bgr] signalling. *Nature* **2013,** *499* (7458), 306-311.
13. Song, W., Fhu, Chee Wai, Ang, Koon Hwee, Liu, Cheng Hao, Johari, Nurul Azizah Binte, Lio, Daniel, Abraham, Sabu, Hong, Wanjin, Moss, Stephen E., Greenwood, John, Wang, Xiaomeng, The fetal mouse metatarsal bone explant as a model of angiogenesis. *Nat. Protocols* **2015,** *10* (10), 1459-1473.
14. Zhang, J., Zhu, L., Fang, J., Ge, Z., Li, X., LRG1 modulates epithelial-mesenchymal transition and angiogenesis in colorectal cancer via HIF-1alpha activation. *Journal of experimental & clinical cancer research : CR* **2016,** *35*, 29-40.
15. Wang, C.-H., Li, Min, Liu, Li-Li, Zhou, Ruo-Yao, Fu, Jia, Zhang, Chris Zhiyi, Yun, Jing-Ping, LRG1 expression indicates unfavorable clinical outcome in hepatocellular carcinoma. *Oncotarget* **2015,** *6* (39), 42118-42129.
16. Bonoiu, A. C., Bergey, E. J., Ding, H., Hu, R., Kumar, R., Yong, K. T., Prasad, P. N., Mahajan, S., Picchione, K. E., Bhattacharjee, A., Ignatowski, T. A., Gold nanorod--siRNA induces efficient in vivo gene silencing in the rat hippocampus. *Nanomedicine (Lond)* **2011,** *6* (4), 617-30.
17. Zheng, D., Giljohann, David A., Chen, David L., Massich, Matthew D., Wang, Xiao-Qi, Iordanov, Hristo, Mirkin, Chad A., Paller, Amy S., Topical delivery of siRNA-based spherical nucleic acid nanoparticle conjugates for gene regulation. *Proceedings of the National Academy of Sciences* **2012,** *109* (30), 11975-11980.
18. Shen, J., Kim, H. C., Mu, C., Gentile, E., Mai, J., Wolfram, J., Ji, L. N., Ferrari, M., Mao, Z. W., Shen, H., Multifunctional gold nanorods for siRNA gene silencing and photothermal therapy. *Adv Healthc Mater* **2014,** *3* (10), 1629-37.
19. Joo, H. N.; Seo, Y. J., A novel gold-based molecular beacon for probing CNG DNA repeat sequences. *Tetrahedron Letters* **2015,** *56* (3), 542-545.
20. Dubertret, B., Calame, Michel, Libchaber, Albert J., Single-mismatch detection using gold-quenched fluorescent oligonucleotides. *Nat Biotech* **2001,** *19* (4), 365-370.
21. Yeo, D. C., Wiraja, Christian, Paller, Amy S., Mirkin, Chad A., Xu, Chenjie, Abnormal scar identification with spherical-nucleic-acid technology. *Nature Biomedical Engineering* **2018,** *2* (4), 227-238.
22. Randeria, P. S., Seeger, M. A., Wang, X. Q., Wilson, H., Shipp, D., Mirkin, C. A., Paller, A. S., siRNA-based spherical nucleic acids reverse impaired wound healing in diabetic mice by ganglioside GM3 synthase knockdown. *Proceedings of the National Academy of Sciences of the United States of America* **2015,** *112* (18), 5573-8.
23. Wu, X. A., Choi, Chung Hang J., Zhang, Chuan, Hao, Liangliang, Mirkin, Chad A., Intracellular Fate of Spherical Nucleic Acid Nanoparticle Conjugates. *Journal of the American Chemical Society* **2014,** *136* (21), 7726-7733.
24. Barnaby, S. N.; Sita, T. L.; Petrosko, S. H.; Stegh, A. H.; Mirkin, C. A., Therapeutic applications of spherical nucleic acids. *Cancer treatment and research* **2015,** *166*, 23-50.
25. Wen, Y.; Pei, H.; Wan, Y.; Su, Y.; Huang, Q.; Song, S.; Fan, C., DNA nanostructure-decorated surfaces for enhanced aptamer-target binding and electrochemical cocaine sensors. *Analytical chemistry* **2011,** *83* (19), 7418-23.
26. Zheng, J.; Zhu, G.; Li, Y.; Li, C.; You, M.; Chen, T.; Song, E.; Yang, R.; Tan, W., A Spherical Nucleic Acid Platform Based on Self-Assembled DNA Biopolymer for High-Performance Cancer Therapy. *ACS Nano* **2013,** *7* (8), 6545-6554.

27. Seftor, E. A.; Seftor, R. E.; Weldon, D. S.; Kirsammer, G. T.; Margaryan, N. V.; Gilgur, A.; Hendrix, M. J., Melanoma tumor cell heterogeneity: a molecular approach to study subpopulations expressing the embryonic morphogen nodal. *Seminars in oncology* **2014,** *41* (2), 259-66.
28. Prigodich, A. E.; Randeria, P. S.; Briley, W. E.; Kim, N. J.; Daniel, W. L.; Giljohann, D. A.; Mirkin, C. A., Multiplexed Nanoflares: mRNA Detection in Live Cells. *Analytical chemistry* **2012,** *84* (4), 2062-2066.
29. Pan, W.; Zhang, T.; Yang, H.; Diao, W.; Li, N.; Tang, B., Multiplexed Detection and Imaging of Intracellular mRNAs Using a Four-Color Nanoprobe. *Analytical Chemistry* **2013,** *85* (21), 10581-10588.
30. Seferos, D. S.; Giljohann, D. A.; Hill, H. D.; Prigodich, A. E.; Mirkin, C. A., Nano-Flares: Probes for Transfection and mRNA Detection in Living Cells. *Journal of the American Chemical Society* **2007,** *129* (50), 15477-15479.
31. Na, L.; Chenyang, C.; Wei, P.; Bo, T., A Multicolor Nanoprobe for Detection and Imaging of Tumor-Related mRNAs in Living Cells. *Angewandte Chemie International Edition* **2012,** *51* (30), 7426-7430.
32. Cutler, J. I.; Auyeung, E.; Mirkin, C. A., Spherical Nucleic Acids. *Journal of the American Chemical Society* **2012,** *134* (3), 1376-1391.
33. Kim, T.; Zhang, Q.; Li, J.; Zhang, L.; Jokerst, J. V., A Gold/Silver Hybrid Nanoparticle for Treatment and Photoacoustic Imaging of Bacterial Infection. *ACS Nano* **2018,** *12* (6), 5615-5625.
34. McKenzie, J. A.; Fruttiger, M.; Abraham, S.; Lange, C. A.; Stone, J.; Gandhi, P.; Wang, X.; Bainbridge, J.; Moss, S. E.; Greenwood, J., Apelin is required for non-neovascular remodeling in the retina. *The American journal of pathology* **2012,** *180* (1), 399-409.
35. Tual-Chalot, S.; Allinson, K. R.; Fruttiger, M.; Arthur, H. M., Whole mount immunofluorescent staining of the neonatal mouse retina to investigate angiogenesis in vivo. *Journal of visualized experiments : JoVE* **2013,** (77), e50546.
36. Salvucci, O.; Ohnuki, H.; Maric, D.; Hou, X.; Li, X.; Yoon, S. O.; Segarra, M.; Eberhart, C. G.; Acker-Palmer, A.; Tosato, G., EphrinB2 controls vessel pruning through STAT1-JNK3 signalling. *Nature Communications* **2015,** *6*, 6576.
37. Hurst, S. J.; Lytton-Jean, A. K. R.; Mirkin, C. A., Maximizing DNA Loading on a Range of Gold Nanoparticle Sizes. *Analytical chemistry* **2006,** *78* (24), 8313-8318.
38. Oberdorster, G.; Oberdorster, E.; Oberdorster, J., Nanotoxicology: an emerging discipline evolving from studies of ultrafine particles. *Environmental health perspectives* **2005,** *113* (7), 823-39.
39. Fischer, H. C.; Chan, W. C., Nanotoxicity: the growing need for in vivo study. *Current opinion in biotechnology* **2007,** *18* (6), 565-71.
40. Saito, K.; Tanaka, T.; Kanda, H.; Ebisuno, Y.; Izawa, D.; Kawamoto, S.; Okubo, K.; Miyasaka, M., Gene expression profiling of mucosal addressin cell adhesion molecule-1+ high endothelial venule cells (HEV) and identification of a leucine-rich HEV glycoprotein as a HEV marker. *Journal of immunology (Baltimore, Md. : 1950)* **2002,** *168* (3), 1050-9.
41. Stahl, A.; Connor, K. M.; Sapieha, P.; Chen, J.; Dennison, R. J.; Krah, N. M.; Seaward, M. R.; Willett, K. L.; Aderman, C. M.; Guerin, K. I.; Hua, J.; Löfqvist, C.; Hellström, A.; Smith, L. E. H., The Mouse Retina as an Angiogenesis Model. *Investigative Ophthalmology & Visual Science* **2010,** *51* (6), 2813-2826.

42. Oh, E.; Delehanty, J. B.; Sapsford, K. E.; Susumu, K.; Goswami, R.; Blanco-Canosa, J. B.; Dawson, P. E.; Granek, J.; Shoff, M.; Zhang, Q.; Goering, P. L.; Huston, A.; Medintz, I. L., Cellular Uptake and Fate of PEGylated Gold Nanoparticles Is Dependent on Both Cell-Penetration Peptides and Particle Size. *ACS Nano* **2011,** *5* (8), 6434-6448.

For TOC only: